symmetry

MDPI

Article

# Axisymmetric Arc Sliding Method of Basal Heave Stability Analysis for Braced Circular Excavations

**Mingju Zhang**[†]**, Zhenbo Zhang**[†]**, Zheng Li**[†] **and Pengfei Li** [*,†]

Key Laboratory of Urban Security and Disaster Engineering, Ministry of Education, Beijing University of Technology, Beijing 100124, China; zhangmj@bjut.edu.cn (M.Z.); zzb759619047@126.com (Z.Z.); zheng.li@bjut.edu.cn (Z.L.)

* Correspondence: lpf@bjut.edu.cn; Tel.: +86-152-1058-3858

† These authors contributed equally to this work.

Received: 4 May 2018; Accepted: 19 May 2018; Published: 22 May 2018

**Abstract:** On the basis of the circular arc sliding model of the limit equilibrium method, an axisymmetric arc sliding method (AASM) is proposed to analyze the basal heave stability of braced circular excavations. The proposed method considers the stiffness of the enclosure structure and spatial effects. The AASM was applied to check basal heave stability in a design example and provided results that were more reasonable than those obtained using other methods. The radii effects in theory and numerical simulation, and the enclosure structure stiffness effects on the basal heave stability safety factor were discussed. Additionally, the effects of the embedded depth on the basal heave stability of a braced circular excavation were analyzed. The safety factor of basal heave stability for a braced circular excavation will be larger when calculated with the AASM than when calculated with the circular arc sliding method, and the optimized embedded depth of the enclosure structure may therefore be reduced by 4∼5 m to lower the cost of the enclosure structure.

**Keywords:** braced circular excavations; basal heave stability; spatial effects; circular arc sliding model; enclosure structure

## 1. Introduction

Many excavations have a circular cross-section in urban construction. As examples, the excavation of the large foundation pit of one skyscraper in Shanghai had a circular cross-section [1], one of the main circular excavations of Thames Water's Lee Tunnel project is the largest excavation in the United Kingdom [2], and a circular excavation was conducted for an underground cylindrical three-dimensional (3D; i.e., having multiple levels) garage [3].

The process of excavation design involves analysis of basal heave stability. There are generally two methods of checking basal heave stability: the bearing capacity theory method and the circular arc sliding method (CASM). Both the bearing capacity theory method and CASM are limit equilibrium methods. With regard to the bearing capacity theory method, Terzaghi [4] provided a formula for the calculations of checking basal heave stability based on bearing capacity theory but the formula is limited to shallow excavations and clay [4]. Later, on the basis of Terzaghi's method, Bjerrum provided formulae for the checking of basal heave stability but these formulae are also limited to clay [5]. With regard to the CASM, many researchers have studied how to obtain reasonable parameters and analyzed the effects of parameters, such as soil parameters, the width of excavation and the embedded depth of the diaphragm wall, on basal heave stability [6].

A limit analysis method has been applied for the analysis of basal heave stability. The formulae for checking basal heave stability were obtained from limit analysis, then the formulae were applied to check the basal heave stability, and the result of the limit analysis method is much more accurate than that of the limit equilibrium method in many cases [7]. The effects of factors and parameters were analyzed [8]. In all the methods cited above, a homogeneous soil assumption is adopted. In addition, under this assumption, the uncertainties in soil properties will be ignored. Futher, uncertainties in soil properties can arise because of limited site investigations, limited soil laboratory tests, and in situ tests, as well as inaccurate correlations for various soil parameters. Also, uncertainties in soil properties stems from spatial variability. To overcome the problems of uncertainties in soil properties, many studies on the reliability analysis of basal heave stability were carried out using the circular arc sliding model. Most of the studies investigated uncertain factors of the soil and newly established methods were applied to practical engineering [9–14]. Reliability analysis for basal heave stability in wide excavations has been discussed on the basis of the bearing capacity theory model and circular arc sliding model. The results obtained using the circular arc sliding model are much more conservative than the results obtained using the bearing capacity theory model [15]. The above methods (i.e., the bearing capacity theory method, circular arc sliding method, limit analysis and reliability analysis) are theoretical methods for the analysis of basal heave stability. Naturally, numerical simulation methods have also been used to calculate the basal heave of excavation. A two-dimensional (2D) model of the finite element method (FEM) was applied to calculate basal heave in an area of soft soil, and four coefficients were introduced to bearing capacity theory [16]. Hashash and Whittle [17] studied the effects of the embedded depth of an enclosure structure, a support structure and the stress history of undrained soil on basal heave stability by numerical simulation [17]. Additionally, three discriminant criterion methods, namely the convergence criterion method, intersection method and angle method, were employed for the 2D model of the FEM with reduced shear strength. Furthermore, the results of an intersection method based on a discriminant criterion of the reduced shear strength are the closest to the results of the bearing capacity theory method and circular arc sliding method as conventional methods [18].

The algorithms of the bearing capacity theory method, circular arc sliding method, limit analysis and reliability analysis are plane-based algorithms. However, circular excavation has self-stability because of its spatial effects. For circular excavation, hoop stress $\sigma_\theta$ was introduced to modify the earth pressure as the first (i.e., maximum) main stress and used to check basal heave stability [19]. In early, some calculation models consider constant cohesion of the soil mass. Cohesion of the soil mass has thus been modified according to the depth of soil in the model. A limit analysis method was then applied to calculate the basal heave stability safety factor for unsupported vertical circular excavations [20,21].

The shear strength reduction method (SSRM) has been used to check basal heave stability. This method adopts an elastoplastic constitutive relationship for the soil, and basal heave failure curves of circular excavation have been obtained [22–26]. Meanwhile, a centrifuge model and full-scale field test have been introduced for the stability of circular excavations.

Although researchers have used many methods to check basal heave stability, the spatial effects of the excavation and enclosure structure have been often ignored. Especially for circular excavations, the constraints of the adjacent soil are strong because hoop stress affects the soil. Circular excavation therefore has spatial effects and self-stability. For the same excavation depth, the lateral deformations of the enclosure structure in circular excavation are smaller than those in rectangular excavation. If a plane algorithm is used to calculate the basal heave stability safety factor of a circular excavation, the embedded depth of the enclosure structure will be so large that the enclosure structure will cost much more.

In this paper, on the basis of the circular arc sliding model of the limit equilibrium method, an axisymmetric arc sliding method (AASM) which is developed based on CASM is proposed to check the basal heave stability of circular excavations. The AASM considers the effects of both the stiffness and deformation of the enclosure structure and the hoop stress on the sliding of soil. AASM has the advantage that it can reflect the spatial effect in the basal heave stability analysis.

## 2. Proposed Axisymmetric Arc Sliding Method—AASM

### *2.1. Problem Description*

The CASM is a well-known method applied to basal heave stability. This method defines the basal heave stability safety factor as the resistance moment divided by the driving moment, Equation (1):

$$k_s = \frac{M_r}{M_s} \tag{1}$$

where, $M_r$ is the resistance moment; $M_s$ is the driving moment; and $k_s$ is the basal heave stability safety factor.

The circular arc sliding model is shown in Figure 1. In the figure, $H$ is the depth of excavation; $D$ is the embedded depth of enclosure structure; $q$ is the ground overload; $O'$ is the center of sliding circular arc; $R$ is the radius of excavation; $R_s$ is the radius of sliding arc; surface ABCE is sliding surface; and UOZ is coordinate system. The following assumptions are made:

(a) Soil slides alone the sliding surface ABCE, on which the shear stress provides the resistance moment
(b) The constitutive relationship of soil can be modeled using Mohr-Coulomb model;
(c) The term $2c\tan(\pi/4 - \varphi/2)$ can be ignored in the active earth pressure formula and the term $2c\tan(\pi/4 + \varphi/2)$ can be ignored in the passive earth pressure formula;
(d) The spatial effects on the soil below the bottom can be ignored.

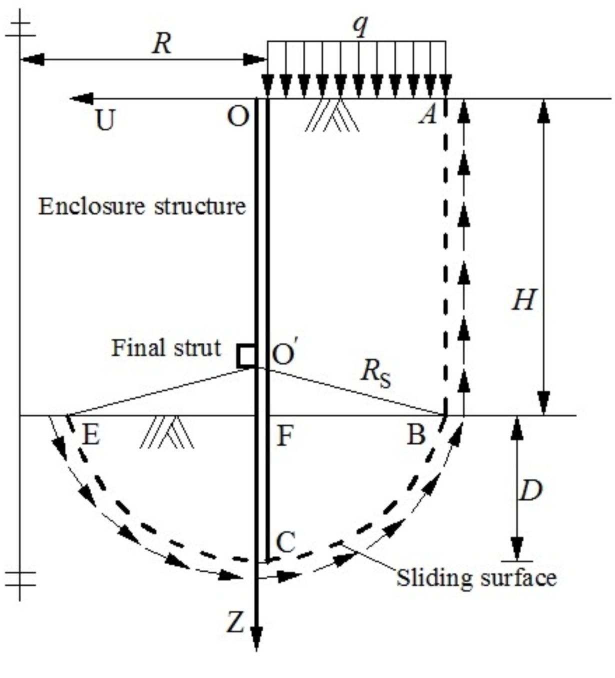


**Figure 1.** Circular Arc Sliding Model.

According to the assumption (a), the resistance moment $M_r$ is generated by the shear stress on the sliding surface AB, BC, CE and braced structure, thus:

$$M_r = M_1 + M_2 + M_3 + M_h \tag{2}$$

where, $M_1$ is the resistance moment generated by shear stress on the sliding surface AB; $M_2$ is the resistance moment generated by shear stress on the sliding surface BC; $M_3$ is the resistance moment generated by shear stress on the sliding surface CE, and $M_h$ is the resistance moment generated by the braced structure. $M_h$ is 800 kN·m for a concrete-braced structure and 600 kN·m for steel-braced structure.

According to the assumption (b), the shear stress is expressed as:

$$\tau = \sigma \tan(\varphi) + c \quad (3)$$

where, $\sigma$ is the normal stress, $\tau$ is the shear stress, $c$ is the cohesion, and $\varphi$ is the friction angle.

The CASM model is derived on a 2D plane. Compared to FEM results, the CASM method gives relative conservative results for circular excavation with an appreciable spatial effect. CASM is a analytical method with reasonable physical meaning and more concise, which could be easily applied in the engineering practice.

AASM was proposed with parabolic deformation form of enclosure structure which is idealized deformation form of enclosure structure [27]. On the basis of the CASM model, the AASM is proposed with reasonable deformation form of enclosure structure so as to obtain a reasonable basal heave stability safety factor for circular excavation considering the spatial effect.

*2.2. Formula of Axisymmetric Arc Sliding Method—AASM*

In this section, the derivation of the formula of AASM is presented. $M_1$ is the resistance moment generated by shear stress on the sliding surface AB, see Figure 2. $L$ is the lateral distance between the sliding surface and the enclosure structure; $u_z$ is the deformation of the enclosure structure at the depth of $z$.

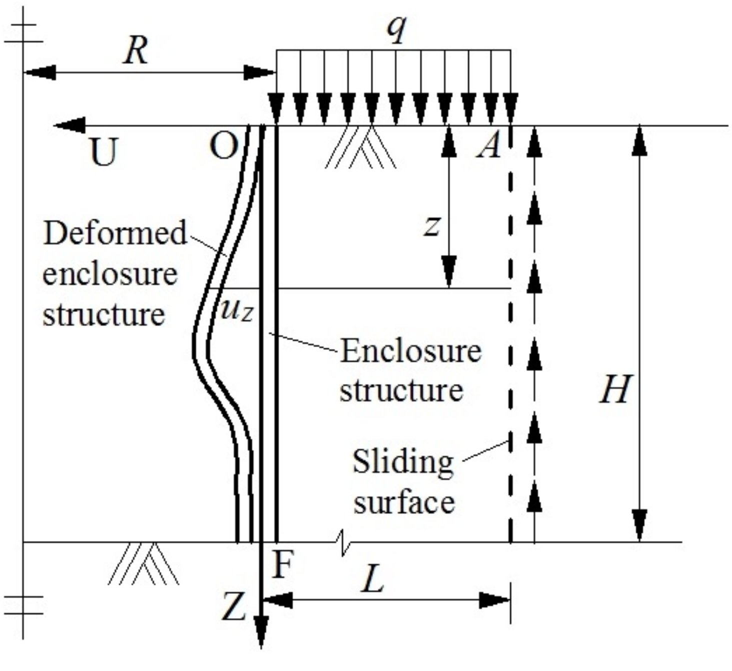


**Figure 2.** Calculation of $M_1$.

The model is built under axisymmetric condition, and the model in Figure 2 is that of the axisymmetric cross-section. The projection of the sliding surface AB on the horizontal plane is a circle as shown Figure 3. There are many plane at any point as shown in Figure 3. For example, planes a-a, b-b, c-c, d-d are all through a point which is in the projection of the sliding surface AB on the horizontal plane. The vertical shear stress is generated in those planes and the maximum vertical shear stress is generated by hoop stress. This shear stress is therefore chosen for calculating the $M_1$.

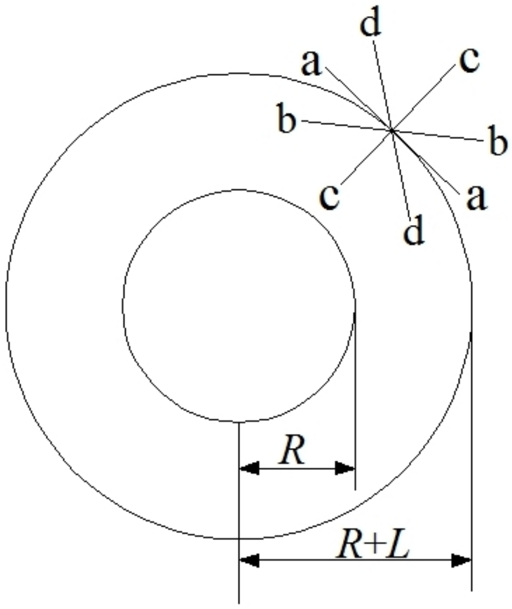


**Figure 3.** Projection of the Sliding Surface AB on the horizontal Plane.

The resistance moment $M_1$ generated on the sliding surface AB can be expressed by the integral formula:

$$M_1 = \int_0^H \tau L dz = \int_0^H (\sigma_\varphi \tan(\varphi) + c) L dz \quad (4)$$

where, $\sigma_\varphi$ is the hoop stress at the depth of $z$ and its calculating diagram is shown in Figure 4. $R_1$ is the internal radius; $\rho$ is the radius of any cross section; $R_2$ is the external radius; $q_1$ is the pressure on the internal circular arc; and $q_2$ is the pressure on the external circular arc.

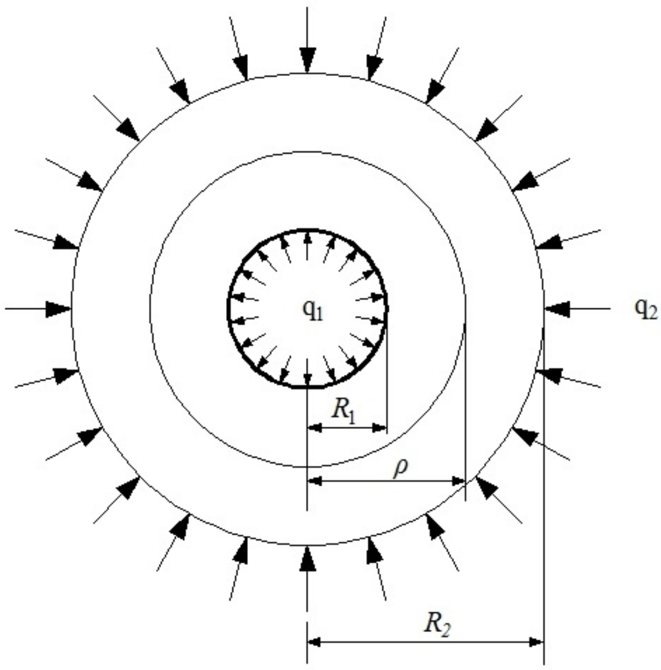


**Figure 4.** Calculation of $\sigma_\varphi$.

The stress solution to the hollow cylinder can be obtained through elastic mechanics and the hoop stress on any cross section is:

$$\sigma_\varphi = [(\frac{R_2^2}{\rho^2} + 1)/(\frac{R_2^2}{R_1^2} - 1)]q_1 - [(1 + \frac{R_1^2}{\rho^2})/(1 - \frac{R_1^2}{R_2^2})]q_2 \tag{5}$$

where, the tensile stress is stipulated to be positive value.

The effects of circular excavation on the surrounding soil are spatially limited. If it is assumed that $R_2$ equals $3R_1$, the pressure on the external circular arc can be considered to be the static earth pressure, i.e.,

$$q_2 = k_0(\gamma z + q) \tag{6}$$

where, $k_0$ is the coefficient of lateral earth pressure at rest ($k_0 = 1 - \sin\varphi$) and $\gamma$ is the soil unit weight.

Taking the deformation of the enclosure structure into consideration, the pressure $q_1$ acting on the internal circular arc can be obtained using the elastic foundation beam method as:

$$q_1 = k_d u_z \tag{7}$$

$$k_d = \frac{E_d b}{R_0^2} \tag{8}$$

where, $k_d$ is the equivalent stiffness of the enclosure structure; $b$ is the thickness of the enclosure structure; $R_0$ is the radius of the enclosure structure; and $E_d$ is the circumferential comprehensive compression modulus of the enclosure structure. Here, $E_d = 0.5 \sim 0.7E$, where $E$ is the elastic modulus of the enclosure structure and $E_d$ should be taken a small value when the $R_0$ is large.

The form of the deformation distribution of the enclosure structure is complicated in practical engineering. However, there are four basic forms, namely the rotational deformation form around the top, rotational deformation form around the bottom, parallel movement form and parabolic deformation form, as shown in Figure 5. $u_1$ is the maximum lateral deformation in the rotational form around the top; $u_2$ is the maximum lateral deformation in the rotational form around the bottom; $u_3$ is the lateral deformation in the parallel movement form; $u_4$ is the maximum lateral deformation in the parabolic deformation form. The deformations of enclosure structure can be expressed as:

$$u_t = \frac{u_1}{(D+H)}z \tag{9a}$$

$$u_b = u_2 - \frac{u_2}{(D+H)}z \tag{9b}$$

$$u_c = u_3 \tag{9c}$$

$$u_p = -\frac{4u_4}{(D+H)^2}z^2 + \frac{4u_4}{(D+H)}z \tag{9d}$$

$$u_z = u_t + u_b + u_c + u_p \tag{9e}$$

where $u_t$ is the lateral deformation in the rotational form around the top at the depth of $z$; $u_b$ is the lateral deformation in the rotational around the bottom at the depth of $z$; $u_c$ is the lateral deformation in the parallel movement at the depth of $z$; and up is the lateral deformation in the parabolic deformation form at the depth of $z$.

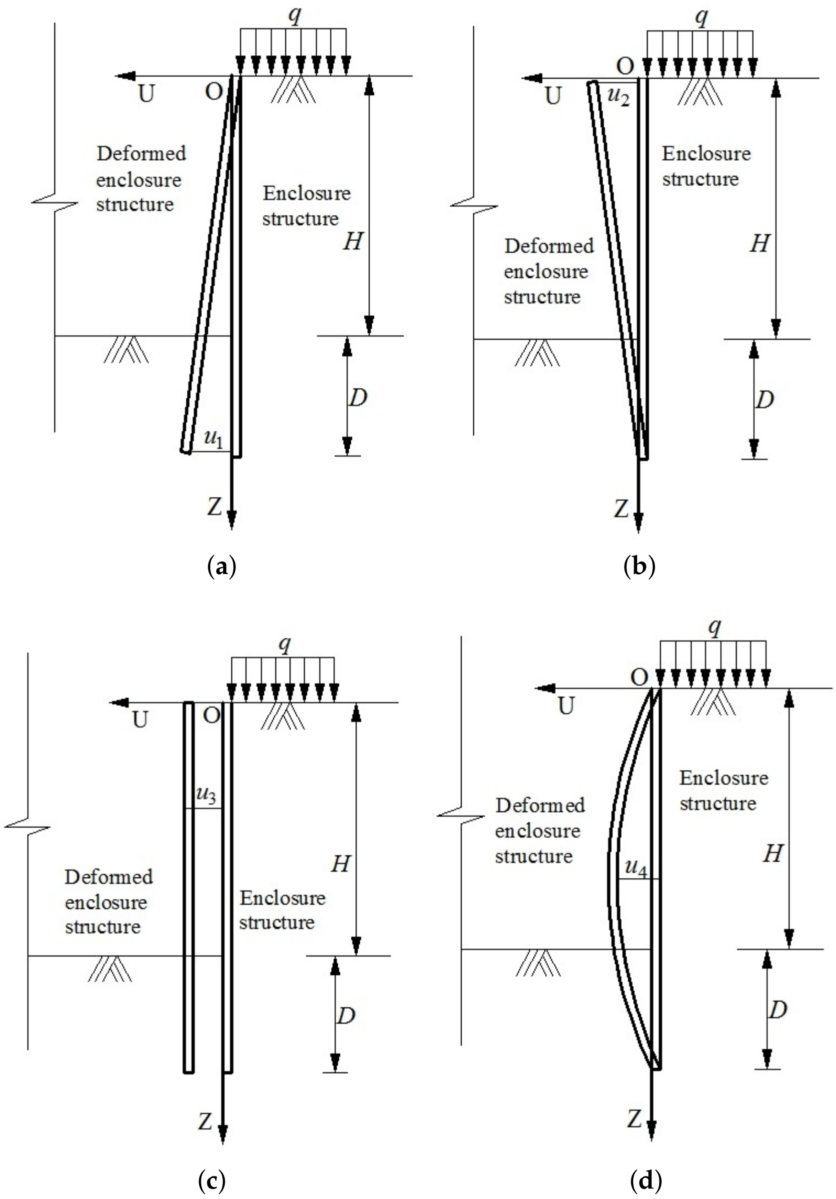


**Figure 5.** Four Basic Displacement patterns of Enclosure Structure, (**a**) Rotation around the Top; (**b**) Rotation around Bottom; (**c**) horizontal translation (**d**) Parabolic Displacement shape.

Substituting the expressions of Equations (5)∼(9) into Equation (4) leads to:

$$\begin{aligned} M_1 &= k_1(1-\sin\varphi)(\frac{\gamma H^2}{2}+qH)L\tan\varphi \\ &+k_2\left[\frac{4u_4+u_1-u_2}{(D+H)}\frac{H^2}{2}-\frac{4u_4}{3(D+H)^2}H^3+(u_2+u_3)H\right]Lk_d\tan\varphi \\ &+cLH \end{aligned} \tag{10}$$

where, $k_1=\left(\frac{9}{8}+\frac{9R^2}{8(R+L)^2}\right)$, $k_2=-\left[\frac{9R^2}{8(R+L)^2}+\frac{1}{8}\right]$

The deformation distribution of the enclosure structure is an important factor in the AASM and its reasonable form shall be obtained from the experience of designers or the results of design software and numerical simulation.

$M_2$ and $M_3$ are respectively the resistance moments generated by shear stress on sliding surfaces BC and CE, and their calculations are illustrated as Figure 6.

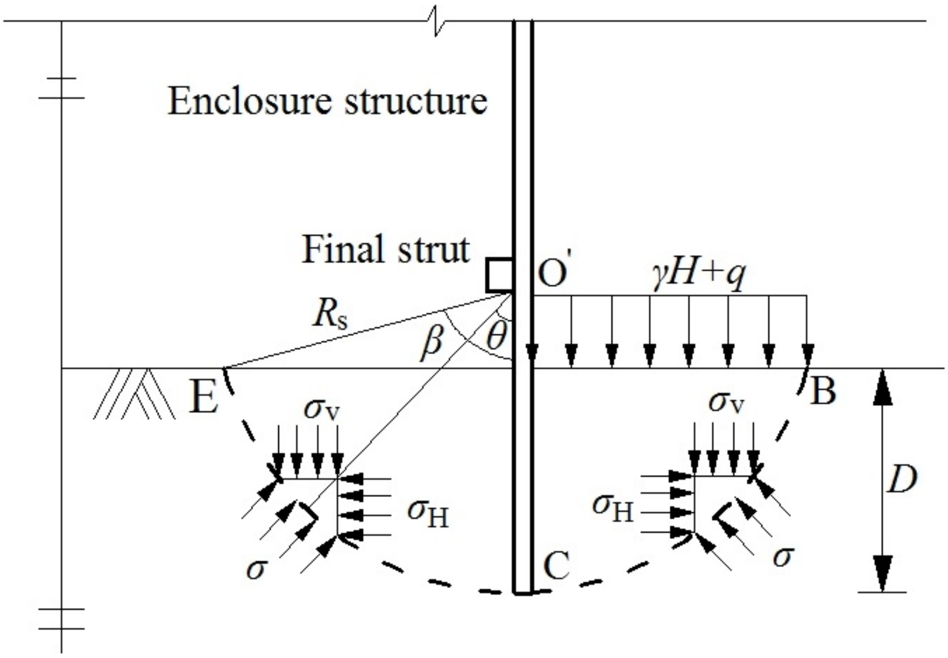


**Figure 6.** Calculation of $M_2$ and $M_3$.

The resistance moment $M_2$ generated on the sliding surface BC can be expressed by the equations:

$$\sigma = \sigma_v \cos\theta + \sigma_H \sin\theta \tag{11a}$$

$$\sigma_V = \gamma(R\cos\theta - R_s + D) + q + \gamma H \tag{11b}$$

$$\sigma_H = k_a \sigma_V \tag{11c}$$

where, $k_a$ is is the active earth pressure factor and here $k_a = \tan^2(\pi/4 - \varphi/2)$.

Accordingly, the resistance moment $M_2$ on sliding surface BC can be derived by the integral calculus:

$$\begin{aligned} M_2 &= \int_0^\beta \tau R_s^2 d\theta \\ &= [\gamma R_s(\frac{\sin 2\beta}{4} + \frac{\beta}{2}) + (\gamma D - \gamma R_s + q + \gamma H)\sin\beta \\ &+ \frac{1}{4}\gamma R_s(1 - \cos 2\beta)k_a + (\gamma D - \gamma R_s + q + \gamma H)(1 - \cos\beta)k_a]R_s^2 \tan\varphi \\ &+ c\beta R_s^2 \end{aligned} \tag{12}$$

The resistance moment $M_3$ generated on the sliding surface CE can be expressed by the equations:

$$\sigma = \sigma_H \sin\theta + \sigma_V \cos\theta \tag{13a}$$

$$\sigma_H = k_p \sigma_V \tag{13b}$$

$$\sigma_V = \gamma(R_s \cos\theta - R_s + D) \tag{13c}$$

where, $k_p$ is the passive earth pressure factor and here $k_p = \tan^2(\pi/4 + \varphi/2)$.

Similarly, the resistance moment $M_3$ on sliding surface CE can be derived by the following equation:

$$\begin{aligned} M_3 &= \int_0^{\beta} \tau R_s^2 d\theta \\ &= [\gamma R_s(\frac{\sin 2\beta}{4} + \frac{\beta}{2}) + \gamma(D - R_s)\sin\beta \\ &+ \frac{1}{4}\gamma R_s(1 - \cos 2\beta)k_p + \gamma(D - R_s)(1 - \cos\beta)k_p]R_s^2 \tan\varphi \\ &+ c\beta R_s^2 \end{aligned} \tag{14}$$

The driving moment $M_s$ is generated by sliding body ABFO in Figure 1, and its formula is expressed as:

$$M_s = \frac{(\gamma H + q)L^2}{2} \tag{15}$$

*2.3. Flowchart and Parameters*

The flow chart for calculating $k_s$ by AASM is shown in Figure 7. In the process of $k_s$ calculation, $M_1$, $M_2$, $M_3$ and $M_h$ are the key parameters that needed to be calculated. For $M_1$, the shear stress on the sliding surface shall be obtained. The shear stress is calculated with the Mohr-Coulomb constitutive relationship, the hoop stress shall be chose as the normal stress in Equation (3). According to the stress solution in the hollow cylinder, the hoop stress can be solved. However, $q_1$ is an important unknown parameter. In addition, $q_1$ could be expressed with the product of enclosure structure stiffness and deformation. The complicated deformation contains four basic forms. Further, the four kinds of maximum lateral deformations of enclosure structure corresponding to four basic forms shall be obtained by the designers' experience or the results of design software and numerical simulation. For $M_2$ and $M_3$, the shear stress on the sliding surface shall be obtained. In addition, the shear stress is obtained with the Mohr-Coulomb soil constitutive relationship, the normal stress shall be obtained by mechanical equilibrium. $M_h$ is obtained according to the design of braced structure.

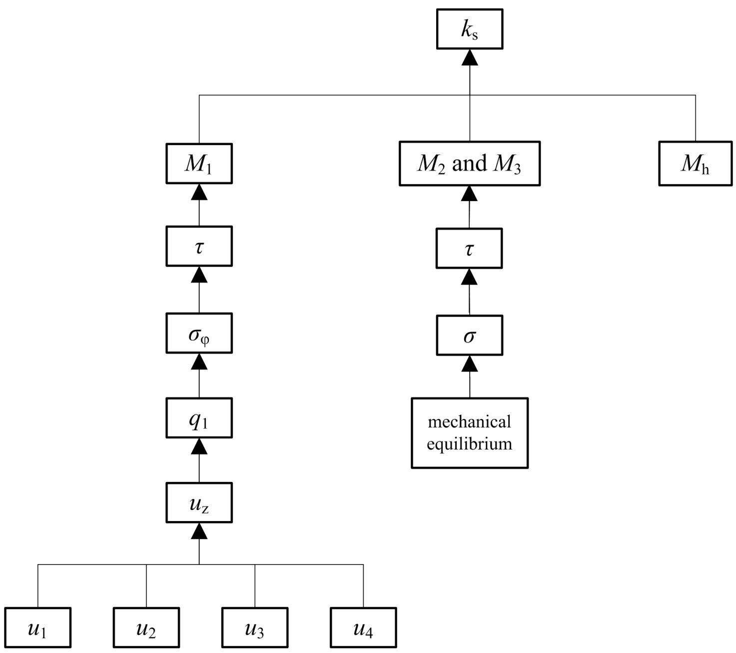


**Figure 7.** Calculation flow chart for $k_s$.

## 3. Case Example

In this section, a case example is presented to illustrated the application of proposed AASM method. The process to obtain some key parameters is presented in details hereafter.

### 3.1. Example Parameters

A circular excavation with diameter of 13.5 m and depth 25 m is designed for an underground cylindrical 3D garage and the field geological compositions and their physical and mechanical parameters are shown in Table 1. The enclosure structure is composed by the piles with the diameter of 1200 mm and with the depth of 40 m, the embedded depth is 15 m and the corresponding central angle of the adjacent pile is 9°. Five ring braces with the cross section of 1500 × 1000 mm are planned to set up and the elevation of ring braces are −1 m, −5 m, −10 m, −15 m and −20 m respectively.

**Table 1.** Properties of soils.

| Soils | Depth $h$(m) | Unit Weight $\gamma$(kN/m$^3$) | Friction Angle $\varphi$( °) | Cohesion $c$(kPa) | Poisson Ratio $\nu$ | Elastic Modulus $E$(MPa) |
|---|---|---|---|---|---|---|
| Silt Plain Fill | 1.5 | 20.5 | 12 | 5 | 0.3 | 5.0 |
| Silt | 2.0 | 19.5 | 25 | 16 | 0.3 | 30.0 |
| Cohesive Soil | 2.0 | 19.6 | 16 | 28 | 0.3 | 40.0 |
| Silt | 1.5 | 19.5 | 25 | 16 | 0.3 | 30.0 |
| Cohesive Soil | 1.5 | 19.6 | 16 | 28 | 0.3 | 40.0 |
| Medium Coarse Sand | 6.0 | 20.0 | 28 | 8 | 0.3 | 75.0 |
| Cohesive Soil | 4.0 | 19.6 | 16 | 28 | 0.3 | 40.0 |
| Silt | 3.0 | 19.5 | 25 | 16 | 0.3 | 30.0 |
| Coarse Sand | 38.5 | 20.0 | 32 | 8 | 0.3 | 120.0 |

$c$ and $\varphi$ are parameters for undrained strength of soils.

### 3.2. Result of $k_s$

The deformation distribution of enclosure structure $u_z$ is an important factor in the AASM. In addition, its reasonable form shall be obtained by the designers' experience or the results of design software and numerical simulation. In this design example, the $u_z$ is obtained by FEM.

The model shown in Figure 8 is constructed by establishing the parts and material properties, assembling the parts, setting the calculation steps including setting the load, and meshing the parts. In terms of establishing parts, axisymmetric parts are chosen. In terms of establishing material properties, a Mohr–Coulomb relationship is taken as the constitutive relationship of the soil. Material parameters of the soil are given in Table 1. The material of the enclosure structure is C30 reinforced concrete having a Poisson ratio of 0.2 and elastic modulus of 25 GPa. The ground overload is set at 20 kPa. The seed density of soil is 1 m in the meshed parts.

In this computation example, the deformation distribution of enclosure structure is obtained by the calculation results of numerical simulation. In addition, the calculation results of enclosure structure deformation distribution are shown in Table 2. Afterwards, through fitting the results of enclosure structure deformation distribution, the parameters are obtained by Equation (9), that is $u_1$ = 2.731 mm, $u_2$ = 0.181 mm, $u_3$ = 0.226 mm, and $u_4$ = 0.269. The basal heave stability safety factors are 2.985 and 3.179, calculated with CASM and AASM respectively for this computation example.

The AASM, in contrast to the CASM, considers not only spatial effects but also the stiffness and deformation of the enclosure structure. The results of basal heave stability safety factors obtained using the AASM are therefore higher than those obtained using the CASM.

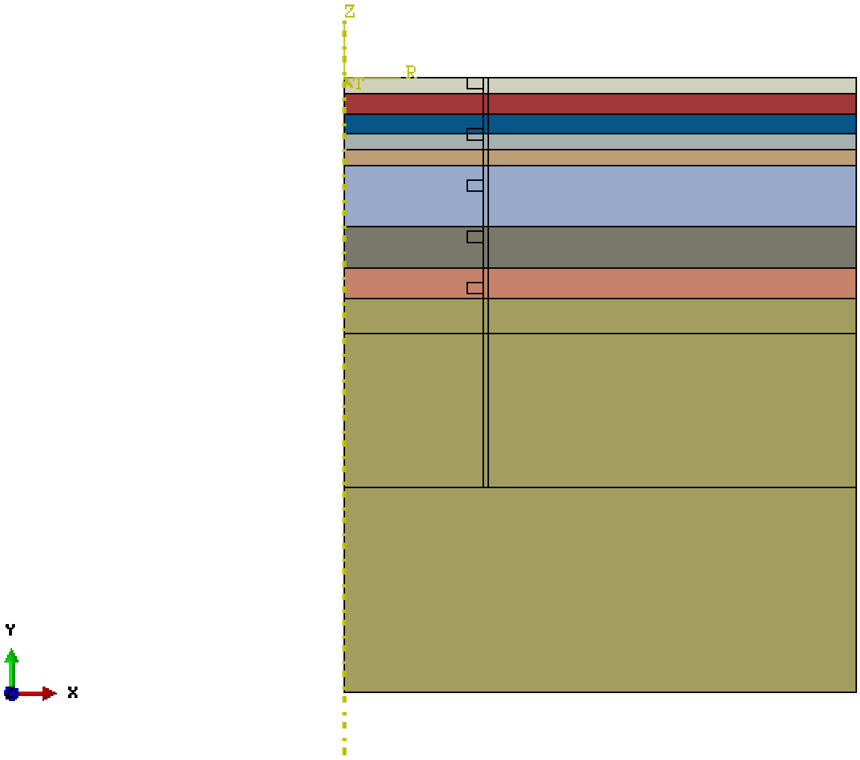


**Figure 8.** FEM model.

**Table 2.** Calculation results of enclosure structure deformation distribution.

| Depth (m) | Displacement of Enclosure Structure (mm) | Depth (m) | Displacement of Enclosure Structure (mm) |
|---|---|---|---|
| 0 | 0.352741 | 22 | 0.686298 |
| 2 | −0.276168 | 24 | 1.13677 |
| 4 | 0.189827 | 26 | 0.156006 |
| 6 | 0.0371271 | 28 | 0.0382515 |
| 8 | 0.512734 | 30 | 0.289966 |
| 10 | 0.39358 | 32 | 0.569906 |
| 12 | 0.599284 | 34 | 0.818515 |
| 14 | 1.0116 | 36 | 1.05388 |
| 16 | 0.446988 | 38 | 1.35405 |
| 18 | 1.76905 | 40 | 2.69007 |
| 20 | 0.81065 | | |

## 4. Parametric Analysis

The model of the AASM is the same as that of the CASM, and the change in the basal heave stability safety factor with a change in soil parameters (referred to as the regularity) is therefore the same for the two methods. Regularity has been well studied and the results are not repeated in this paper.

### 4.1. Radius Effect on $k_s$ in the Theoretical Solution

The AASM considers both the stiffness and deformation of the enclosure structure and the hoop stress effects on the sliding face. The parameter effect of the excavation radius is therefore analyzed.

The $k_s$ results of 6 different radius excavations were discussed. The process of calculation with AASM is the same as the above process. The deformation distribution of the enclosure structure $u_z$ in excavations of different radii is obtained using the FEM as shown in Figure 9. Then, through fitting the results of enclosure structure deformation distribution in those different radius excavations, the parameters are obtained in Equation (9).

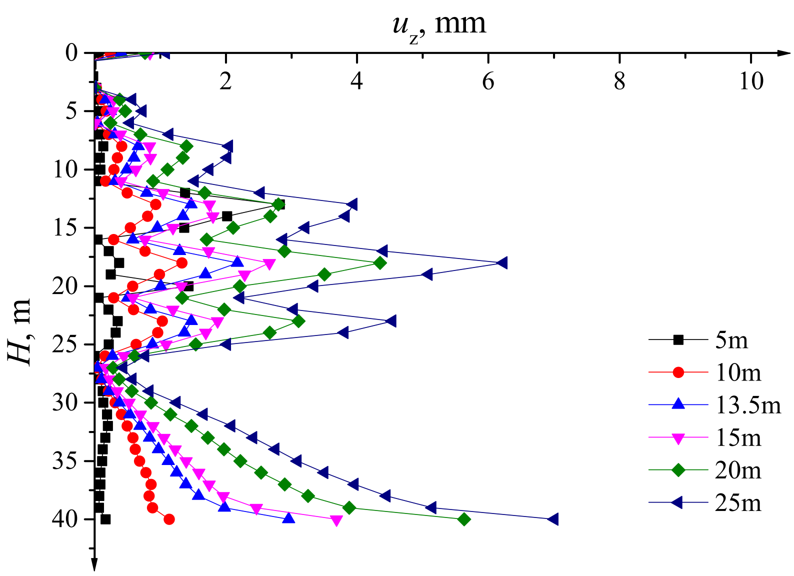


**Figure 9.** $u_z$ in different radius excavations.

The effects of the excavation radius on the basal heave stability safety factors obtained using the CASM and AASM are shown in Figure 10. With increasing excavation radius, the basal heave stability safety factor obtained using the CASM does not change because the CASM ignores spatial effects. However, the basal heave stability safety factor obtained using the AASM decreases with an increasing excavation radius because the AASM considers the beneficial spatial effects of the excavation radius.

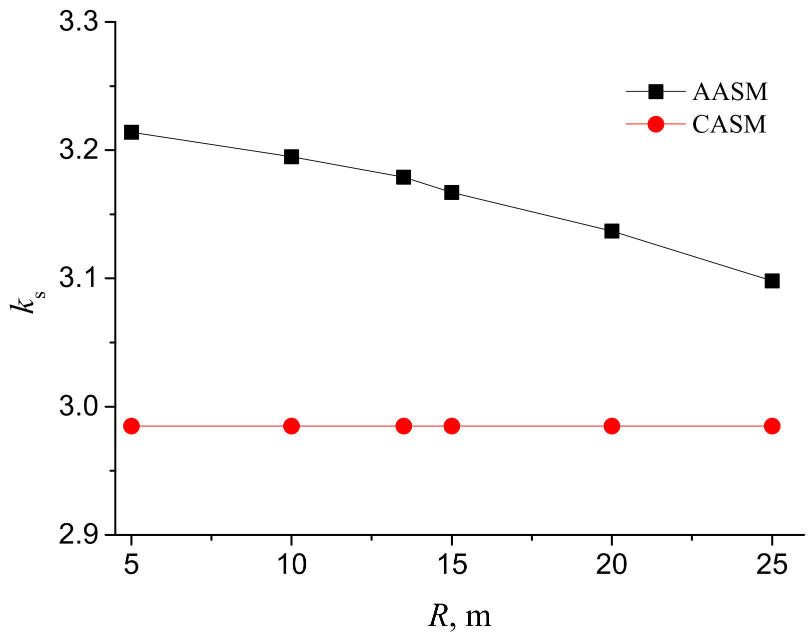


**Figure 10.** Excavation Radius Effect on AASM and CASM.

### 4.2. Radius Effect on $k_s$ in the Numerical Simulation

The excavation basal heave obtained using 2D and 3D FEMs in the excavations of six different radii are shown in Figure 11. The excavation basal heave is chosen to reflect the effect of the radius on the basal heave stability safety factor qualitatively. Additionally, with an increasing excavation radius, the excavation basal heave decreases rapidly according to the 3D FEM because the beneficial spatial effects rapidly weaken with increasing excavation radius. However, the excavation basal heave decreases in the 2D FEM slowly because the 2D FEM ignores the spatial effects.

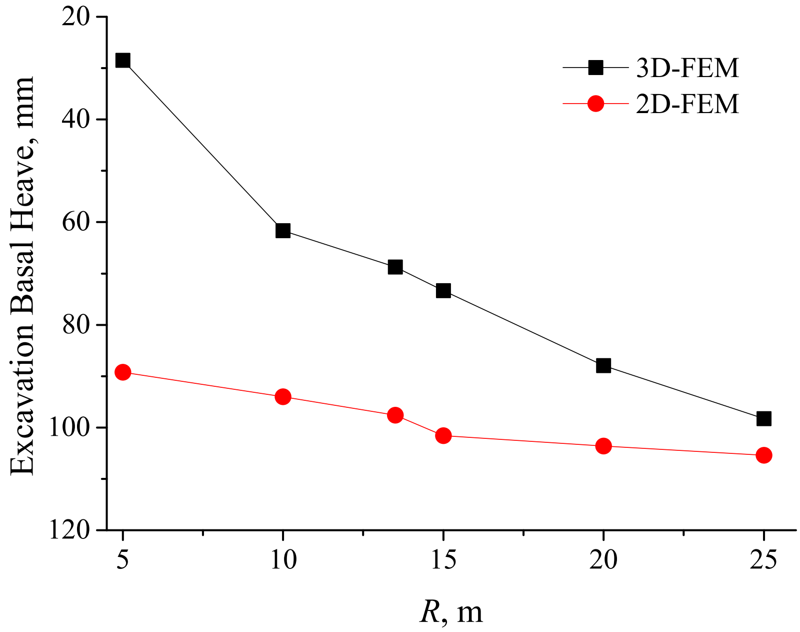


**Figure 11.** Excavation Radius Effect on 2D and 3D FEM.

Overall, the excavation basal heave does not reflect the effect of the radius on the basal heave stability safety factor. 2D and 3D SSRMs are chosen to calculate the safety factors of basal heave stability for different radii of excavation. In these SSRMs, the safety factor of basal heave stability is defined as:

$$k_s = \frac{c + \sigma \tan \varphi}{c' + \sigma \tan \varphi'} \tag{16}$$

where, $c'$ and $\varphi'$ are the reduced cohesive and reduced friction angle respective when the excavation basal heave is unstable.

The intersection method is chose as convergence criterion method [18]. Figure 12 shows the typical nodal deformation versus $k_s$ curve. The typical nodal deformation increases slowly at the beginning, but then developed rapidly. The slow curve and the rapid curve will intersect at intersection point. The corresponding $k_s$ value is regarded as the basal heave stability safety factor.

The SSRM was applied to calculate the design computed example, and the results were shown in Figure 13. With an increasing excavation radius, the safety factor of basal heave stability obtained using the 2D SSRM hardly changes whereas that obtained using the 3D SSRM decreases. Spatial effects are considered in the 3D SSRM but ignored in the 2D SSRM. This is the reason that the above results of the 2D and 3D SSRMs appear regular.

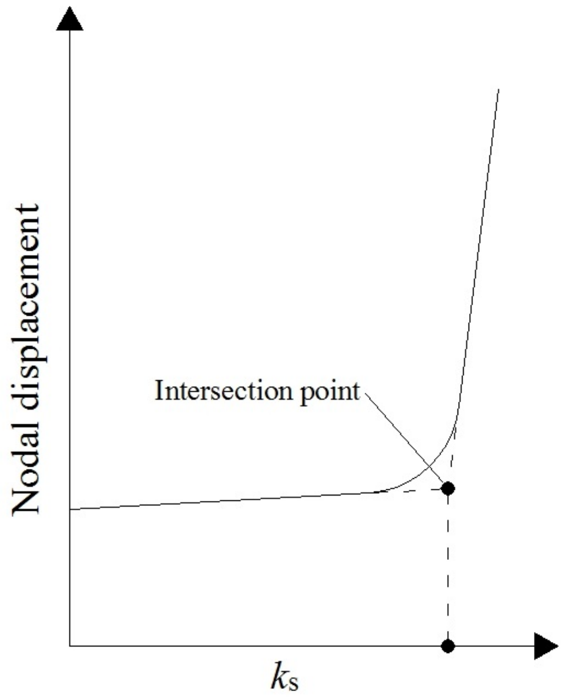


**Figure 12.** Node displacement vs. $k_s$ curve, after Do et al. [18].

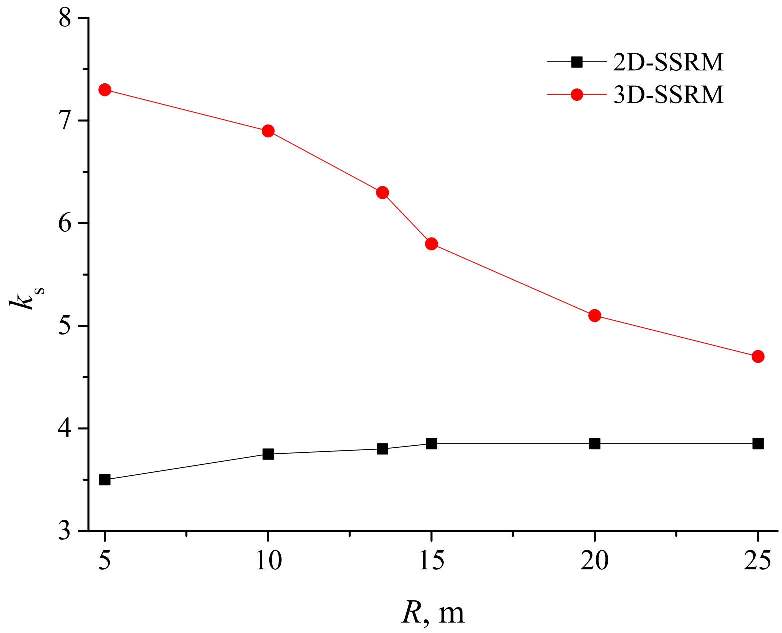


**Figure 13.** Calculation Results by SSRM.

### *4.3. Enclosure Structure Stiffness Effect on $k_s$*

The design example has a pile diameter of 1200 mm. Five diameters of the pile are considered in analyzing the effect of the enclosure structure stiffness on $k_s$. The calculation process of the AASM is the same as the process described above. Deformation distributions of the enclosure structure $u_z$ for the different diameters of pile obtained using the FEM are shown in Figure 14. By fitting the results of the distribution of the enclosure structure deformation, the parameters in Equation (9) are obtained.

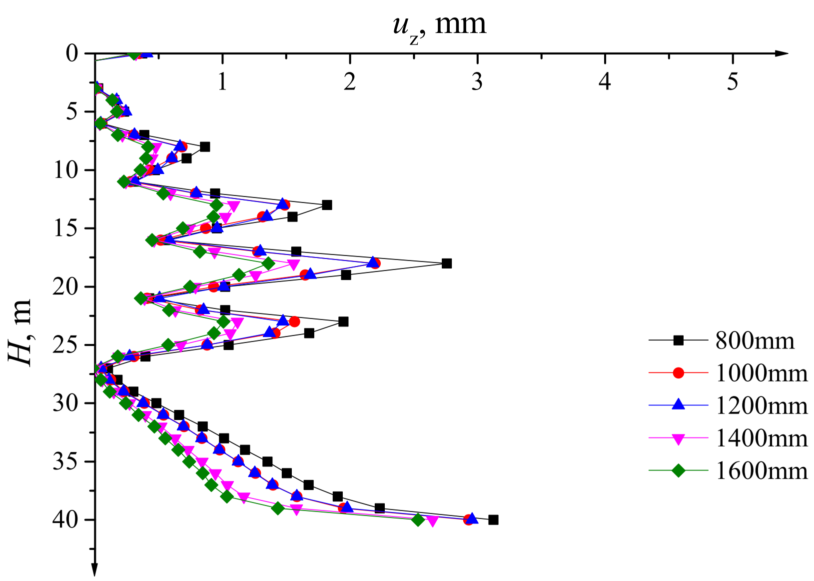


**Figure 14.** $u_z$ in different diameters of piles.

Effects of the enclosure structure stiffness on the safety factors of basal heave stability obtained using the CASM and AASM are shown in Figure 15. The excavation basal heaves obtained using the 3D FEM are given in Table 3. With increasing stiffness of the enclosure structure, the safety factors of basal heave stability obtained using the CASM and AASM and the excavation basal heaves obtained using the 3D FEM do not change. However, the explanations differ for the two methods. In the case of the CASM, the stiffness of the enclosure structure is ignored. In the case of the AASM, with increasing stiffness of the enclosure structure, the deformation of the enclosure structure increases and $q_1$ in the AASM does not change. In the 3D FEM, the enclosure structure is rigid and the sliding surface does not change.

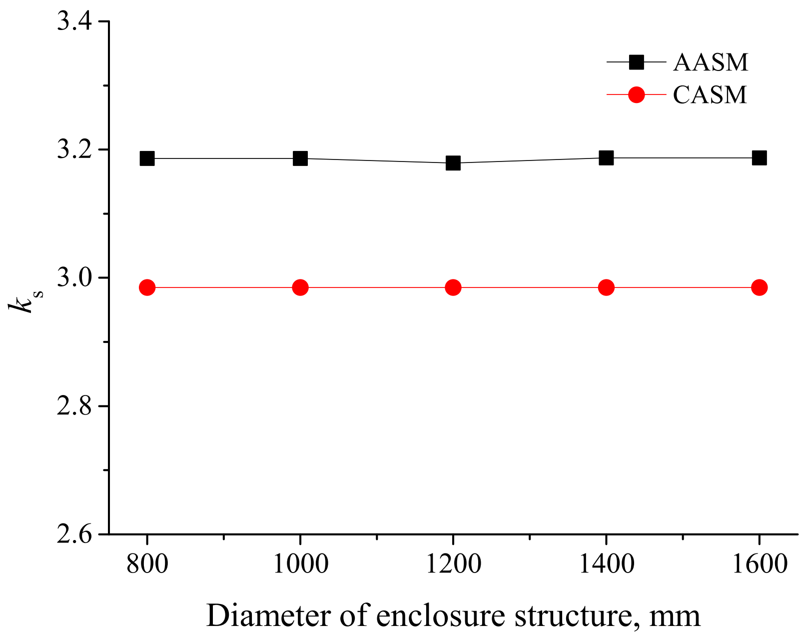


**Figure 15.** Effect of enclosure structure stiffness.

**Table 3.** Results of excavation basal heave with 3d SSRM.

| Diameter of pile (mm) | 800 | 1000 | 1200 | 1400 | 1600 |
|---|---|---|---|---|---|
| Excavation basal heave (mm) | 63.89 | 63.55 | 63.27 | 63.01 | 62.75 |

### 4.4. Embedded Depth Effect on $k_s$

The embedded depth of the enclosure structure is 15 m in the design example. Eight embedded depths of the enclosure structure are considered for analysis of the effect of the embedded depth on $k_s$. The calculation process of the AASM is the same as the process described above. The deformation distributions of the enclosure structure $u_z$ for the different embedded depths obtained using the FEM are shown in Figure 16. By fitting the results of the distribution of the enclosure structure deformation, the parameters in Equation (9) are obtained.

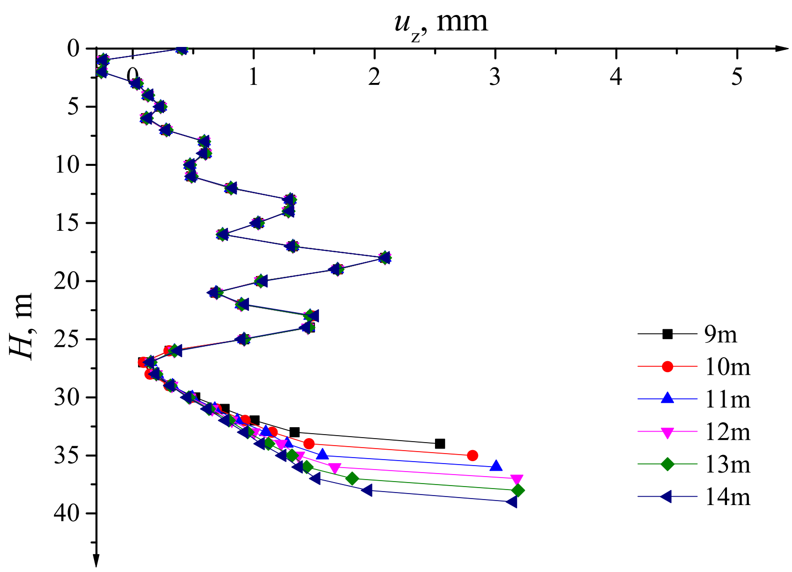


**Figure 16.** $u_z$ in different embedded depth.

The parameter effects of the embedded depth are analyzed; calculation results are given in Table 4. The obtained results are obtained using the CASM and AASM for different embedded depths. In the case of circular excavation, if the safety factors of basal heave stability are the same, the embedded depth of the enclosure structure may be optimized in terms of reducing the cost of the enclosure structure. The embedded depth of the enclosure structure may be reduced by 4∼5 m.

**Table 4.** Results of different embedded depths.

| **Embedded Depth (m)** | **CASM** | **AASM** |
|---|---|---|
| 9 | 2.742 | 2.969 |
| 10 | 2.760 | 2.977 |
| 11 | 2.791 | 3.000 |
| 12 | 2.830 | 3.034 |
| 13 | 2.876 | 3.076 |
| 14 | 2.928 | 3.126 |
| 15 | 2.985 | 3.189 |
| 16 | 3.045 | 3.241 |

## 5. Conclusions

A new method (i.e., the AASM) was developed on the basis of the circular arc sliding model. However, when the radius of excavation is smaller than the radius of the sliding circular arc (i.e., the sliding circular arc intersects both sides of the cross-section of the excavation), the sliding soil surface under the excavation may change and this new method should be modified. The main results of this study are as follows:

(1) The AASM combines stiffness with deformation of the enclosure structure to check the basal heave stability of circular excavations and considers spatial effects.
(2) The basal heave stability safety factor calculated with the AASM is higher than that calculated with the CASM. A design example demonstrates that the AASM results are reasonable.
(3) A computation example revealed that, in the case of circular excavation, if basal heave stability safety factors are the same, the embedded depth of the enclosure structure may be reduced by 4$\sim$5 m to lower the cost of the enclosure structure.

**Author Contributions:** Conceptualization and Methodology, M.Z.; Software, Z.Z.; Validation, Z.L.; Investigation and Supervision, P.L.

**Acknowledgments:** The authors would like to acknowledge the financial support from the Collaborative Innovation Project of Chaoyang District, Beijing (XC1402), National Natural Science Foundation of China (51538001) and Beijing Natural Science Foundation (8161001), and technical support from Innovative Research Team of Beijing University of Technology.

**Conflicts of Interest:** The authors declare no conflict of interest.

## References

1. Tan, Y.; Wang, D.L. Structural Behaviors of Large Underground Earth-Retaining Systems in Shanghai. II: Multipropped Rectangular Diaphragm Wall. *J. Perform. Constr. Facil.* **2015**, *29*, 4014059, doi:10.1061/(ASCE)CF.1943-5509.0000535. [CrossRef]
2. Schwamb, T.; Soga, K.; Mair, R.J.; Elshafie, M.Z.E.B.; Sutherden, R.; Boquet, C.; Greenwood, J. Fibre optic monitoring of a deep circular excavation. *Proc. Inst. Civ. Eng. Geotech. Eng.* **2014**, *167*, 144–154. [CrossRef]
3. Zhang, M.J.; Zhang, Z.B.; Du, X.L. Research on Number of Car Elevators for Cylindrical Underground Garage Based on Queuing Theory. *China J. Highw. Transp.* **2017**, *30*, 133–139.
4. Terzaghi, K. *Theoretical Soil Mechanics*; John Willey and Sons: New York, NY, USA, 1943; pp. 118–143.
5. Bjerrum, L.; Eide, O. Stability of strutted excavations in clay. *Géotechnique* **1956**, *6*, 32–47. [CrossRef]
6. Zheng, G.; Cheng, X.S. Basal stability analysis method considering arc length and normal stress correction. *Chin. J. Geotech. Eng.* **2012**, *34*, 781–789.
7. Chang, M.F. Basal stability analysis of braced cuts in clay. *J. Geotech. Geoenviron. Eng.* **2000**, *126*, 276–279. [CrossRef]
8. Ukritchon, B.; Whittle, A.J.; Sloan, S.W. Undrained Stability of Braced Excavations in Clay. *J. Geotech. Geoenviron. Eng.* **2003**, *129*, 738–755. [CrossRef]
9. Goh, A.T.C.; Kulhawy, F.H.; Wong, K.S. Reliability assessment of Basal-Heave stability for braced excavations in clay. *J. Geotech. Geoenviron. Eng.* **2008**, *134*, 145–153. [CrossRef]
10. Wu, S.H.; Ou, C.Y.; Ching, J.; Hsein Juang, C. Reliability-Based Design for Basal Heave Stability of Deep Excavations in Spatially Varying Soils. *J. Geotech. Geoenviron. Eng.* **2012**, *138*, 594–603. [CrossRef]
11. Luo, Z.; Atamturktur, S.; Cai, Y.; Juang, C.H. Reliability analysis of basal-heave in a braced excavation in a 2-D random field. *Comput. Geotech.* **2012**, *39*, 27–37. [CrossRef]
12. Luo, Z.; Atamturktur, S.; Cai, Y.; Juang, C.H. Simplified Approach for Reliability-Based Design against Basal-Heave Failure in Braced Excavations Considering Spatial Effect. *J. Geotech. Geoenviron. Eng.* **2012**, *138*, 441–450. [CrossRef]
13. Fan, L.; Wu, Z.; Wan, Z.; Gao, J.W. Experimental investigation of thermal effects on dynamic behavior of granite. *Appl. Therm. Eng.* **2017**, *125*, 94–103. [CrossRef]
14. Wu, Z.; Fan, L.F.; Liu, Q.; Ma, G.W. Micro-mechanical modeling of the macro-mechanical response and fracture behavior of rock using the numerical manifold method. *Eng. Geol.* **2017**, *225*, 49–60. [CrossRef]

15. Wu, S.H.; Ou, C.Y.; Ching, J. Reliability based design of base heave dtability in wide excavations. In *Geo-Risk 2011: Risk Assessment and Management*; American Society of Civil Engineers: Reston, VA, USA, 2011; pp. 680–687.
16. Goh, A.T.C. Estimating basal-heave stability for braced excavations in soft clay. *J. Geotech. Eng.* **1994**, *120*, 1430–1436. [CrossRef]
17. Hashash, Y.M.A.; Whittle, A.J. Ground Movement Prediction for Deep Excavations in Soft Clay. *J. Geotech. Eng.* **1996**, *122*, 474–486. [CrossRef]
18. Do, T.N.; Ou, C.Y.; Asce, M.; Lim, A. Evaluation of Factors of Safety against Basal Heave for Deep Excavations in Soft Clay Using the Finite-Element Method. *J. Geotech. Geoenviron. Eng.* **2013**, *139*, 2125–2135. [CrossRef]
19. Wang, H. Stability Analysis of Retaining Structure for Circular Foundation Pit. *Chin. J. Undergr. Space Eng.* **2011**, *7*, 1653–1659.
20. Khatri, V.N.; Kumar, J. Stability of an unsupported vertical circular excavation in clays under undrained condition. *Comput. Geotech.* **2010**, *37*, 419–424. [CrossRef]
21. Kumar, J.; Chakraborty, M.; Sahoo, J.P. Stability of Unsupported Vertical Circular Excavations. *J. Geotech. Geoenviron. Eng.* **2014**, *140*, 4014028, doi:10.1061/(ASCE)GT.1943-5606.0001118. [CrossRef]
22. Cai, F.; Ugai, K.; Hagiwara, T. Base Stability of Circular Excavations in Soft Clay. *J. Geotech. Geoenviron. Eng.* **2002**, *128*, 702–706. [CrossRef]
23. Faheem, H.; Cai, F.; Ugai, K.; Hagiwara, T. Two-dimensional base stability of excavations in soft soils using FEM. *Comput. Geotech.* **2003**, *30*, 141–163. [CrossRef]
24. Faheem, H.; Cai, F.; Ugai, K. Three-dimensional base stability of rectangular excavations in soft soils using FEM. *Comput. Geotech.* **2004**, *31*, 67–74. [CrossRef]
25. Goh, A.T. Basal heave stability of supported circular excavations in clay. *Tunn. Undergr. Space Technol.* **2017**, *61*, 145–149. [CrossRef]
26. Kim, K.Y.; Lee, D.S.; Cho, J.; Jeong, S.S.; Lee, S. The effect of arching pressure on a vertical circular shaft. *Tunn. Undergr. Space Technol.* **2013**, *37*, 10–21. [CrossRef]
27. Zhang, M.J.; Zhang, Z.B.; Yang, M. A Three-Dimensional Axisymmetric Arc Sliding Method for Checking Basal Heave Stability of Circular Foundation Pits. In *Proceedings of the 2nd International Symposium on Asia Urban GeoEngineering*; Chen, R., Zheng, G., Ou, C., Eds.; Springer: Singapore, 2018; pp. 116–124.